Title

Quantification of the Hemodynamic Changes of Cirrhosis with Free-Breathing Self-Navigated MRI

Journal

Journal of Magnetic Resonance Imaging, 53(5)

ISSN

1053-1807

Authors

Brunsing, Ryan L
Brown, Dustin
Almahoud, Hashem
et al.

Publication Date

2021-05-01

DOI

10.1002/jmri.27488

Peer reviewed

HHS Public Access

Author manuscript

J Magn Reson Imaging. Author manuscript; available in PMC 2022 June 02.

Published in final edited form as:

J Magn Reson Imaging. 2021 May ; 53(5): 1410–1421. doi:10.1002/jmri.27488.

Quantification of the Hemodynamic Changes of Cirrhosis with Free-Breathing Self-Navigated MRI

Ryan L. Brunsing, MD, PhD,
Department of Radiology, Stanford University, Palo Alto, CA

Dustin Brown, MD, PhD,
Department of Radiology, University of California, San Diego, La Jolla, CA

Hashem Almahoud, MD,
Department of Radiology, University of California, San Diego, La Jolla, CA

Yuko Kono, MD,
Division of Gastroenterology, Department of Medicine, University of California, San Diego, La Jolla, CA

Rohit Loomba, MD,
Division of Gastroenterology, Department of Medicine, University of California, San Diego, La Jolla, CA

Irene Vodkin, MD,
Division of Gastroenterology, Department of Medicine, University of California, San Diego, La Jolla, CA

Claude B. Sirlin, MD,
Department of Radiology, University of California, San Diego, La Jolla, CA

Marcus T. Alley, PhD,
Department of Radiology, Stanford University, Palo Alto, CA

Shreyas S. Vasanawala, MD, PhD,
Department of Radiology, Stanford University, Palo Alto, CA

Albert Hsiao, MD, PhD
Department of Radiology, University of California, San Diego, La Jolla, CA

Abstract

Background: Non-invasive assessment of the hemodynamic changes of cirrhosis could help guide therapeutic development and clinical management of these patients.

Purpose: To determine whether free-breathing 4D flow MRI with self-navigation can assess the hemodynamic changes in cirrhosis.

Study Type: Retrospective.

(corresponding author): hsiao@ucsd.edu.

Field Strength / Sequence: 3T / free-breathing time-resolved three-directional velocity encoding MRI with soft gating and golden-angle view ordering.

Assessment: Measurements of the supra-celiac abdominal aorta (SCA), supra-renal abdominal aorta (SRA), celiac trunk (CeT), superior mesenteric artery (SMA), splenic artery (SpA), common hepatic artery (CHA), portal vein (PV), and supra-renal inferior vena cava (IVC) were acquired by two readers. Novel measures of hepatic vascular resistance (hepatic arterial relative resistance, HARR; portal resistive index, PRI) were developed to quantify cirrhosis-related alterations blood flow.

Statistical analysis: Bland-Altman, linear regression, Tukey's multiple comparison test.

Results: 44 of 47 studies yielded measurable data (94%). There was high inter-reader concordance across all measured arterial structures (range; r = 0.948 – 0.987) and the IVC (r = 0.972), with moderate concordance in the PV (r = 0.866). Conservation of mass analysis showed moderate to high concordance between large vessels (SRA vs. IVC; r = 0.806), small vessels (Celiac vs. CHA+SpA; r = 0.939), and across capillary beds (CeT+SMA vs. PV; r = 0.862). There was increased splanchnic flow in patients with portosystemic shunting (PSS) relative to control patients and patients with cirrhosis but without PSS ($p < 0.0001$ across CeT, SpA, and CHA). HARR was elevated and PRI was decreased in patients with PSS compared to both other groups.

Data Conclusion: 4D flow MRI with self-navigation is technically reliable, showing promise for quantitative assessment of the hemodynamic changes in cirrhosis. Novel quantitative metrics of hepatic vascular resistance correlate with PSS.

Summary Statement: Free-breathing, self-navigated 4D flow MRI enables quantification of the hemodynamic changes in cirrhosis, allowing development of quantitative metrics which correlate with altered hepatic and portal blood flow.

Keywords

4Dflow; liver; cirrhosis; splanchnic; portal vein; TIPS

INTRODUCTION

Advanced cirrhosis is associated with a systemic hyperdynamic circulatory syndrome and increased cardiac output (1). These vascular changes contribute to portal hypertension (2) which drives much of the morbidity and mortality associated with cirrhosis (3–6). Reproducible non-invasive assessment of these hemodynamic changes could help guide therapeutic development and clinical management of these patients.

Imaging is attractive for blood flow quantification as it is non-invasive. Doppler ultrasound is commonly used for hepatic vascular assessment in cirrhosis and may be able to detect elevated portal pressures (7). Contrast-enhanced ultrasound has also been studied (8,9). However ultrasound is prone to operator variability (10) and limited field of view. Portosystemic collateral pathways are variable in both size and location, making comprehensive hemodynamic assessment with ultrasound challenging. 2D phase contrast MRI is useful in abdominal imaging (11) and has been validated against Doppler ultrasound

(12), but requires *a priori* plane prescription, which is time consuming and impractical for routine practice.

Phase-contrast magnetic resonance imaging with three-directional velocity encoding and cardiac gating (4D flow) allows for time-resolved quantification of blood flow across any plane, definable before or after the acquisition, within the imaging volume. Major challenges to routine use in abdominal imaging include long scan duration and artifact from respiratory and cardiac motion. Furthermore, in contrast to larger arterial vessels typically interrogated in cardiac imaging, the smaller vessel caliber and slower flow rates of the splanchnic vasculature are more susceptible to motion artifact.

To help address these issues, a single breath-hold technique using spiral trajectories and compressed sensing was developed, however signal-to-noise limitations may impact quantitative reproducibility (13,14). Additionally, breath-hold techniques can fail in patients who cannot reliably hold their breath, as is commonly encountered in patients with liver disease. Multiple other 4D flow techniques have been developed to help mitigate motion in the liver including pencil-beam navigators (15) and highly undersampled 3D radial trajectories (16), which can include incorporation of off-resonance correction (17). Leveraging some of these approaches, 4D flow has been used in preoperative assessment prior to living donor liver transplant(18), to characterize flow dynamics at the splenomesenteric confluence (19), assess transhepatic portosystemic shunt function (15), for risk stratification in gastroesophageal varices (20), as well as qualitative (21) and quantitative (22) evaluation of portal blood flow.

Here we explored a different approach, leveraging a single free-breathing cartesian 4D flow variant utilizing self-navigation and spiral-like view ordering (4D flow-SN), which can be acquired in under 10 minutes. We first perform a technical validation assessing interobserver agreement and conservation of mass across splanchnic arterial and portal venous structures. We then introduce quantitative metrics of hepatic vascular resistance and demonstrate their correlation with the presence of portosystemic shunts, as determined by conventional MRI.

MATERIALS AND METHODS:

Study design:

This single-center retrospective study with cross-sectional and longitudinal components was Health Insurance Portability and Accountability Act compliant and approved by the institutional review board with waiver of informed consent. Consecutive patients who underwent MRI that included 4D flow-SN between October 2015 and June 2017 were identified and enrolled.

Inclusion criteria were; (i) having undergone 4D flow-SN and (ii) concurrent contrast-enhanced diagnostic MRI of the abdomen that, at minimum, included an axial T2-weighted, axial pre- and post-contrast T1-weighted spoiled gradient recalled images, and diffusion weighted images for anatomic evaluation and detection of liver lesions.

Exclusion criteria were; (i) any history of prior vascular surgery in the abdomen or pelvis, (ii) metallic foreign body in the abdomen causing susceptibility artifact which rendered the images uninterpretable, (iii) presence of an IVC filter, (iv) known liver malignancy, or (iv) non-fasting state. For the control cohort (see below), additional exclusion criteria included known liver disease.

Patient classification:

Patients without known liver disease based on review of the electronic medical record were placed in the *control cohort*; and patients with a diagnosis of cirrhosis from a hepatologist as assessed via review of the electronic medical record were referred to as the *cirrhosis cohort*. This group was then further subdivided into those without appreciable portosystemic shunting (*non-PSS cohort*) and those with portosystemic shunting (*PSS cohort*), which could either be biologic (neovascularization) or iatrogenic (such as a transjugular intraheptic portosystemic shunt or TIPS). Assessment for the presence of biologic portosystemic shunting was completed by two authors (---, a 4th year radiology resident, and ---, a 2nd year radiology resident) by reviewing the anatomic imaging for each case. Biologic shunting was defined as vascular collaterals between the portal venous and systemic venous systems measuring at least 5mm in diameter. TIPS were similarly identified. Disagreements were resolved by consensus of the residents and the corresponding author prior to data collection.

4D flow MRI technique:

Examinations were completed on one of two 3T Discovery 750 platforms (GE Healthcare, Milwaukee, Wisconsin) using a 32-channel phased-array coil. Our 4D flow MRI technique used a 3D cartesian strategy in in which (K_y-K_z) samples are grouped in spiral-like sets, which are acquired with golden angle ordering (23,24). Golden angle ordering helps render motion incoherent and evenly spaces sampling over time(25). Dense sampling at the center of k-space allows incorporation of butterfly navigators for soft gating (26) to further aid in motion compensation. This combined technique is referred to as 4D flow with self-navigation (4D flow-SN, see Supplemental Video 1). Images were acquired after the administration of intravenous contrast and following the acquisition of dynamic post contrast imaging. Several different contrast agents were used depending on the study indication (Supplemental Table 1). Velocity encoding (venc) ranged from 80 – 250 cm/s. Data was split into 20 cardiac phases, resulting in a temporal resolution of 29 – 64 ms/phase. Further imaging parameters can be found in Table 1. Example videos are included in the supplemental material.

4D flow MRI analysis:

Using commercially available software (Cardio DL v2.3, Arterys, San Francisco, CA), two radiologists (one fourth year resident (--) and one faculty member with 8 years of experience with 4D flow MRI (--)) independently quantitated blood flow across the abdominal aorta above the celiac trunk (SC aorta) and above the renal arteries (SR aorta), celiac truck, superior mesenteric artery (SMA), splenic artery, common hepatic (CHA) arteries, inferior vena cava above the renal veins (SR IVC) and main portal vein (PV) by drawing triplicate planar regions of interest (ROIs) orthogonal to the direction of blood flow in a single reading session as assessed subjectively using a combination of dynamic color-coded 3D and planar

cine imaging as well as phase maps (Figure 1). Areas of aliasing were excluded from the analysis using phase maps. Background phase error correction was done using this same commercially available software prior to data collection.

Resistive indices:

We calculated two novel metrics of hepatic vasculature resistance, based on an idealized circuit of flow within the splanchnic vasculature. The conceptual underpinning and formula derivations are explained in Figure 2.

The first metric is the hepatic arterial relative resistance (HARR):

$$\frac{splenic\ artery\ flow}{CHA\ flow}$$

The second is a marker of portal vein resistance called the portal resistive index (PRI):

$$\frac{SR\ Aorta\ flow + CHA\ flow}{splenic\ artery\ flow + SMA\ flow}$$

These metrics ignore the inferior mesenteric artery, lumbar arteries, left gastric artery, and gastroduodenal artery, based on the assumption that blood flow in these vessels is comparatively small. These equations do not account for anatomic variants. If an anatomic variant does exist, the equation could be altered accordingly. In our study, one patient has an accessory right hepatic artery off the SMA which was small and not well visualized on 4D flow MRI and was ignored for the sake of simplicity. Another patient had a replaced right hepatic artery off the SMA, which was measured concurrently with the left hepatic artery as they coursed in close proximity to one another near the hepatic hilum. Multiple other patients had accessory left hepatic arteries off the left gastric arteries, which were not well visualized on 4D flow MRI and were ignored for the sake of simplicity.

Statistical analysis

Patient demographics, exam technical adequacy and individual vessel measurability were summarized descriptively. Assessment of interreader variability was done by Bland-Altman analysis and linear regression. Kappa was used to estimate inter-reader agreement on measurability. Comparison of flow metrics between the three patient cohorts (controls, cirrhosis without PSS, and cirrhosis with PSS) was done using Tukey's multiple comparison test. Differences in flow between various subgroup were reported with 95% confidence intervals. Analysis was completed using Excel 2018 (Microsoft, Redmond, WA) and GraphPad Prism v8.2.1 (GraphPad Software, La Jolla, CA).

RESULTS:

Patient cohorts:

Between September 2015 and June 2017, 27 consecutive patients without cirrhosis meeting inclusion criteria were identified. Six were excluded (Figure 3A). This left 21 patients in the control cohort (7 males, 14 females, mean age 50.4 yrs, age range 26–77 yrs).

Over this same time period, 28 consecutive patients with cirrhosis meeting inclusion criteria were identified. Two were excluded (Figure 3B). This left 26 patients with cirrhosis in the study. Among these, 7 patients with native or iatrogenic portosystemic shunting comprise the PSS cohort (2 males, 5 females, mean age 59.9 yrs, age range 33–76 yrs). The 19 remaining patients with cirrhosis but without PSS comprise the non-PSS cohort (11 males, 8 females, mean age 57.3 yrs, age range 20–79 yrs).

Per-patient and per-vessel flow analysis:

In total, 94% (44/47) of cases were technically adequate. Three cases were identified by both readers as technically inadequate, meaning no viable measurements could be obtained from any vessel: one due to motion artifact, malfunction in cardiac-gating or extensive velocity-aliasing each. Two cases occurred in the non-PSS cohort and one case occurred in the PSS cohort.

In all 44 technically adequate cases, the SC aorta, SR aorta, celiac trunk, superior mesenteric artery, and SR IVC were measurable by both readers and showed high inter-reader agreement (Bland-Altman bias ≤0.02 L/m, Pearson's coefficient r = 0.949 – 0.984; Table 2, Figure 4). Both readers deemed the splenic artery measurable in 89% (42/47) of cases with high inter-reader agreement (bias = 0.01 L/m, r = 0.987). Both readers deemed the CHA and PV measurable in 83% (39/47) of cases with high inter-reader agreement for the CHA (bias <0.01 L/m, r = 0.948) and moderate inter-reader agreement for the PV (bias = 0.04 L/m, r = 0.866).

There were a few cases where the readers disagreed on measurability; 2 cases in the splenic artery, 5 cases in the CHA, and 4 cases in the PV. There was substantial agreement between the readers on measurability (365 of 376 patient-vessel combinations, Kappa = 0.804, 95% CI from 0.691 – 0.916).

Conservation of flow analysis:

Flow measurements were compared for conservation of mass (flow continuity) across four distinct vessel combinations. There was high concordance of blood flow across small arterial structures (celiac trunk vs. CHA + splenic artery: bias = 0.106 L/m, r = 0.939; (Table 3). Similarly, there was high concordance between large and small vessels (SC Aorta - SR Aorta vs. celiac trunk + SMA: bias = 0.026 L/m, r = 0.909). There was moderate concordance of flow between large arterial and venous structures (SR aorta vs. SR IVC: bias = 0.034 L/m, r = 0.806) and across capillary beds (PV vs. celiac trunk + SMA: bias = 0.311 L/m, r = 0.862).

Comparative analysis of blood flow in the setting of cirrhosis with and without PSS.

The PSS cohort exhibited increased blood flow into the abdominal aorta (SC aorta) relative to both control ($p < 0.0001$, mean difference 0.91 L/m) and non-PSS populations ($p < 0.0001$, mean difference 1.14 L/m; Table 4, Figure 5). This increased flow was directed to the splanchnic system as flow in the celiac trunk, SMA, splenic artery, CHA, and PV were all significantly higher in the PSS cohort as compared to both other groups ($p < 0.0001$ in all cases; Table 4, Figure 5). In contrast, there was no significant difference in blood flow between the control and non-PSS cohort across any of these vessels (p = 0.11 – 0.95).

Flow within the SR IVC was similar across all cohorts (p = 0.43 – 0.94). Blood flow in the SR aorta was decreased in PSS (p = 0.0026, –0.37 L/m) and non-PSS cohort (p < 0.0001, –0.34 L/m) relative to the control cohort.

Quantitative imaging biomarkers of hepatic blood flow

We developed novel metrics of vasculature resistance, one measuring the hepatic artery resistance ratio (HARR), and one estimating portal venous resistance (PRI). HARR and PRI values were compared across groups (Figure 6). Patients in whom the required measurements were not obtained by either reader were excluded from analysis.

HARR was elevated in the PSS cohort (mean = 3.68, 95% CI 1.76 – 5.61) relative to both the control cohort (mean = 2.11, 95% CI 1.50 – 2.71, p = 0.021) and the non-PSS cohort (mean = 2.16, 95% CI 1.71 – 2.61, p = 0.031). There was no difference between the control and non-PSS cohorts (p = 0.99).

PRI was decreased in the PSS cohort (mean = 1.30, 95% CI 0.88 – 1.71) relative to both the control cohort (mean = 3.18, 95% CI 2.63 – 3.73, p = 0.0003) and the non-PSS cohort (mean = 2.37, 95% CI 1.96 – 2.79, p = 0.040). PRI was also decreased in the non-PSS cohort relative to the control cohort (p = 0.049).

DISCUSSION:

In this work we demonstrate the feasibility and reliability of a free-breathing 4D flow MRI technique with intrinsic motion compensation in quantitative assessment of blood flow in the upper abdomen. The reliability of this technique allowed us to introduce a set of quantitative metrics of hepatic and portal vascular resistance, HARR and PRI, which showed significant changes in the setting of portosystemic shunting.

The combination of spiral-like view ordering with golden-angle permutation and soft gating was able to compensate for respiratory and cardiac motion without the use of external tracking devices. This technique has previously been evaluated in pediatric populations (23,27), but this is the first application to an adult population. Acceleration allowed acquisition of high resolution volumetric 4D flow data over the entire abdomen in 10 minutes. We also simultaneously assessed blood flow in arteries and veins, across both large and small vessels, with substantial inter-reader reproducibility. Conservation of flow analysis and consistency with prior reports suggest our measurement are accurate as well.

The hemodynamic changes of cirrhosis result from increased flow in the hepatic vasculature (2), while blood flow in vascular beds outside the liver is decreased due to functional central hypovolemia (28). We detected a significant decrease in the portal resistive index (PRI) in patients with cirrhosis which occurred in both the PSS and non-PSS cohorts, likely due to decreased blood flow within the aorta below the celiac trunk and SMA (SR Aorta). This is consistent with expected effects of cirrhosis on the peripheral circulation. In addition, we detected increased celiac trunk, splenic artery, and common hepatic artery blood flow in the PSS cohort. These findings are consistent with existing models of the hyperdynamic syndrome of cirrhosis.

Portal hypertension contributes to the morbidity and mortality of cirrhosis, and current catheter-based methods of detection are invasive. There was a significant decrease in portal vein blood flow in the non-PSS cohort, as compared to controls, which may indicate underlying portal hypertension. In comparison to the non-PSS cohort, patients with PSS showed increased portal flow and decreased PRI, as expected (29). Further studies are needed to determine if changes in the flow metrics can reliably predict the presence and resolution of portal hypertension.

Robust MRI-based assessment of splanchnic blood flow may improve our understanding of cirrhosis. These patients often suffer from poor respiratory capacity or irregular breathing, which can undermine the use of external tracking devices and breath hold techniques. In 3 of 47 studies using 4D flow with self-navigation artifact precluded any blood flow measurements, however motion artifact undermined image quality in only once case. In the remaining 44 studies, 90% of the vessels were measurable by both readers, including all 44 aortas, celiac trunks, SMAs, and IVCs. These findings suggest 4D flow with self-navigation is motion robust in the upper abdomen.

Validation of 4D flow MRI techniques can be challenging. 4D flow MRI has been validated against perivascular ultrasound in a porcelain model of portal hypertension (30), but there is no clear gold standard for comparison in patients. Conservation of flow analysis is often used as a surrogate for an external measure of reliability and consistency of blood flow measurements. Our conservation of flow analysis across 4 distinct sets of vasculature all showed moderate to high agreement, and our measurements in good agreement with prior reports (18,20,31). Taken together these data increase confidence that our measurements are accurate.

The ability to measure both arterial and venous flow from a single study has practical clinical implications. The importance of arterial or venous flow may vary over time for a given patient, and there are clinical scenarios where evaluation of both systems is of interest, for example following liver transplant (32). Both readers obtained highly reproducible measurements across multiple vessels in all 44 technically adequate studies. Prior studies have concurrently assessed hepatic arteries and portal veins (13,21,31). In one study (31), inter-observer assessment of the concurrently acquired hepatic artery and portal vein blood flow yielded an average bias of 3% and 10%, respectively, and in another biases ranged from 4.2 – 15.7% for arteries and 7.6% for the portal vein (13). Averaged biases across vessels in this study ranging from less than 1% for the hepatic artery up to 4% for the portal vein. There was also high inter-reader agreement on measurability for individual vessels (97%). Thus, reproducible measurements can be made concurrently in arterial and venous systems using 4D flow with self-navigation.

The ability to reliably assess splenic vascular flow may aid the clinical workup of hypersplenism (33) or serve a role in identification of candidates for partial splenic embolization (34,35). A previously reported 4D flow-based metric termed the splenic flow index was superior to splenic volume and simple blood flow measures in predicting the serological derangements of cirrhosis-associated hypersplenism (36). In this study we detected an increased hepatic arterial resistance ratio (HARR) in patients with PSS, likely

reflecting decreased splenic artery resistance. Further studies will be needed to see if these measures can play a direct role in clinical care.

Quantification of the portal vein wasn't as reliable as other vessels. One option to help address this issue might be time averaging, which has been shown improve measurements in the portal system (22). Time averaging could increase reproducibility of portal measurements in the setting where temporally resolved imaging with a high venc is desired for concurrent arterial assessment. Another option might be a dual venc technique (37), however this is time consuming and may be impractical without further developments in acceleration to help reduce scan time.

Limitations:

This study has several notable limitations. The data was acquired retrospectively. Reliance on conservation of mass analysis may allow technique-related errors in measurement to go undetected and get distributed across all measurements. In particular the quantitative metrics derived here need to be validated against a true gold standard, such as wedge pressures or another invasive metric of vascular flow. There were differences in the number of females across cohorts, which could account for some of the differences observed. There was a larger reader variance in the portal vein, likely due to the slow flow (generally less than 20 cm/s) which is harder to resolve with the higher venc values that are needed to assess the arterial structures. There were only a small number of patients in each cohort, especially the PSS cohort, thus these findings require validation in a larger dataset. Analysis for 4D flow data is time intensive. Thus incorporation into routine clinical workflow will require automated analysis (38), which might be possible with advances in machine learning (39). Small accessory anatomic variant hepatic arteries, which were often not well visualized, were not factored in the analysis under the assumption that their narrow caliber equated to very low blood flows which would have minimal impact on our imaging metrics.

Conclusions:

Free-breathing, self-navigated 4D flow MRI is a motion-robust technique for assessing splanchnic blood flow, enabling accurate and precise quantification of hemodynamic changes in cirrhosis. By assessing both arterial and venous blood supply, quantitative metrics of hepatic resistance can be calculated which correlate with the presence of portosystemic shunting.

Supplementary Material

Refer to Web version on PubMed Central for supplementary material.

Abbreviations:

4D flow-SN	4D flow MRI with self-navigation
CHA	Common hepatic artery
IVC	Inferior vena cava

PSS	Porto-systemic shunting
PV	Main portal vein
SC aorta	Abdominal aorta above the celiac trunk
SR aorta	Abdominal aorta above the renal arteries
SR IVC	Inferior vena cava above the renal veins
SMA	Superior mesenteric artery: SMA
TIPS	Transjugular intrahepatic portosystemic shunt

REFERENCES:

1. Møller S, Bendtsen F. The pathophysiology of arterial vasodilatation and hyperdynamic circulation in cirrhosis. Liver Int. 2018;38(4):570–580. [PubMed: 28921803]
2. Bolognesi M, Di Pascoli M, Verardo A, Gatta A. Splanchnic vasodilation and hyperdynamic circulatory syndrome in cirrhosis. World J Gastroenterol WJG. 2014;20(10):2555–2563. [PubMed: 24627591]
3. Salerno F, Guevara M, Bernardi M, et al. Refractory ascites: pathogenesis, definition and therapy of a severe complication in patients with cirrhosis. Liver Int. 2010;30(7):937–947. [PubMed: 20492521]
4. Thomopoulos K, Theocharis G, Mimidis K, Lampropoulou-Karatza C, Alexandridis E, Nikolopoulou V. Improved survival of patients presenting with acute variceal bleeding. Prognostic indicators of short- and long-term mortality. Dig Liver Dis Off J Ital Soc Gastroenterol Ital Assoc Study Liver. 2006;38(12):899–904.
5. Angeli P, Garcia-Tsao G, Nadim MK, Parikh CR. News in pathophysiology, definition and classification of hepatorenal syndrome: A step beyond the International Club of Ascites (ICA) consensus document. J Hepatol. 2019;71(4):811–822. [PubMed: 31302175]
6. D'Amico G, Garcia-Tsao G, Pagliaro L. Natural history and prognostic indicators of survival in cirrhosis: A systematic review of 118 studies. J Hepatol. 2006;44(1):217–231. [PubMed: 16298014]
7. Zhang L, Yin J, Duan Y, Yang Y, Yuan L, Cao T. Assessment of intrahepatic blood flow by Doppler ultrasonography: Relationship between the hepatic vein, portal vein, hepatic artery and portal pressure measured intraoperatively in patients with portal hypertension. BMC Gastroenterol. 2011;11(1):84. [PubMed: 21767412]
8. Jeong WK, Kim TY, Sohn JH, Kim Y, Kim J. Severe Portal Hypertension in Cirrhosis: Evaluation of Perfusion Parameters with Contrast-Enhanced Ultrasonography. PLOS ONE. 2015;10(3):e0121601.
9. Liu D, Qian L, Wang J, Hu X, Qiu L. Hepatic Perfusion Parameters of Contrast-Enhanced Ultrasonography Correlate With the Severity of Chronic Liver Disease. Ultrasound Med Biol. 2014;40(11):2556–2563. [PubMed: 25218453]
10. Sacerdoti D, Gaiani S, Buonamico P, et al. Interobserver and interequipment variability of hepatic, splenic, and renal arterial Doppler resistance indices in normal subjects and patients with cirrhosis. J Hepatol. 1997;27(6):986–992. [PubMed: 9453423]
11. Burkart DJ, Johnson CD, Ehman RL, Weaver AL, Ilstrup DM. Evaluation of portal venous hypertension with cine phase-contrast MR flow measurements: high association of hyperdynamic portal flow with variceal hemorrhage. Radiology. 1993;188(3):643–648. [PubMed: 8351326]
12. Yzet T, Bouzerar R, Allart J-D, et al. Hepatic vascular flow measurements by phase contrast MRI and doppler echography: A comparative and reproducibility study. J Magn Reson Imaging. 2010;31(3):579–588. [PubMed: 20187200]
13. Bane O, Peti S, Wagner M, et al. Hemodynamic measurements with an abdominal 4D flow MRI sequence with spiral sampling and compressed sensing in patients with chronic liver disease. J Magn Reson Imaging. 0(0)10.1002/jmri.26305. Accessed February 5, 2019.

14. Dyvorne H, Knight-Greenfield A, Jajamovich G, et al. Abdominal 4D Flow MR Imaging in a Breath Hold: Combination of Spiral Sampling and Dynamic Compressed Sensing for Highly Accelerated Acquisition. Radiology. 2014;275(1):245–254. [PubMed: 25325326]
15. Owen JW, Saad NE, Foster G, Fowler KJ. The Feasibility of Using Volumetric Phase-Contrast MR Imaging (4D Flow) to Assess for Transjugular Intrahepatic Portosystemic Shunt Dysfunction. J Vasc Interv Radiol. 2018;29(12):1717–1724. [PubMed: 30396843]
16. Gu T, Korosec FR, Block WF, et al. PC VIPR: A High-Speed 3D Phase-Contrast Method for Flow Quantification and High-Resolution Angiography. Am J Neuroradiol. 2005;26(4):743–749. [PubMed: 15814915]
17. Johnson KM, Lum DP, Turski PA, Block WF, Mistretta CA, Wieben O. Improved 3D Phase Contrast MRI with Off-resonance Corrected Dual Echo VIPR. Magn Reson Med Off J Soc Magn Reson Med Soc Magn Reson Med. 2008;60(6):1329–1336.
18. Rutkowski DR, Reeder SB, Fernandez LA, Roldán-Alzate A. Surgical planning for living donor liver transplant using 4D flow MRI, computational fluid dynamics and in vitro experiments. Comput Methods Biomech Biomed Eng Imaging Vis. 2018;6(5):545–555. [PubMed: 30094106]
19. Rutkowski DR, Medero R, Garcia FJ, Roldán-Alzate A. MRI-based modeling of splenomesenteric confluence flow. J Biomech. 2019;88:95–103. [PubMed: 30928204]
20. Motosugi U, Roldán-Alzate A, Bannas P, et al. Four-dimensional Flow MRI as a Marker for Risk Stratification of Gastroesophageal Varices in Patients with Liver Cirrhosis. Radiology. 2018;290(1):101–107. [PubMed: 30325278]
21. Frydrychowicz A, Landgraf B, Niespodzany E, et al. 4D Velocity Mapping of the Hepatic and Splanchnic Vasculature with Radial Sampling at 3T: A Feasibility Study in Portal Hypertension. J Magn Reson Imaging JMRI. 2011;34(3):577–584. [PubMed: 21751287]
22. Landgraf BR, Johnson KM, Roldán-Alzate A, Francois CJ, Wieben O, Reeder SB. Effect of temporal resolution on 4D flow MRI in the portal circulation. J Magn Reson Imaging. 2014;39(4):819–826. [PubMed: 24395121]
23. Cheng JY, Zhang T, Ruangwattanapaisarn N, et al. Free-Breathing Pediatric MRI with Nonrigid Motion Correction and Acceleration. J Magn Reson Imaging JMRI. 2015;42(2):407. [PubMed: 25329325]
24. Cheng JY, Hanneman K, Zhang T, et al. Comprehensive Motion-Compensated Highly-Accelerated 4D Flow MRI with Ferumoxytol Enhancement for Pediatric Congenital Heart Disease. J Magn Reson Imaging JMRI. 2016;43(6):1355–1368. [PubMed: 26646061]
25. Winkelmann S, Schaeffter T, Koehler T, Eggers H, Doessel O. An Optimal Radial Profile Order Based on the Golden Ratio for Time-Resolved MRI. IEEE Trans Med Imaging. 2007;26(1):68–76. [PubMed: 17243585]
26. Cheng JY, Alley MT, Cunningham CH, Vasanawala SS, Pauly JM, Lustig M. Non-rigid Motion Correction in 3D Using Autofocusing with Localized Linear Translations. Magn Reson Med Off J Soc Magn Reson Med Soc Magn Reson Med. 2012;68(6):1785–1797.
27. Zhang T, Yousaf U, Hsiao A, et al. Clinical performance of a free-breathing spatiotemporally accelerated 3-D time-resolved contrast-enhanced pediatric abdominal MR angiography. Pediatr Radiol. 2015;45(11):1635–1643. [PubMed: 26040509]
28. Wythe S, Davies TW, O'Beirne J, Martin D, Gilbert-Kawai E. Observational study of the microcirculation in patients with liver cirrhosis. JGH Open Open Access J Gastroenterol Hepatol. 2019;3(6):518–524.
29. Bannas P, Roldán-Alzate A, Johnson KM, et al. Longitudinal Monitoring of Hepatic Blood Flow before and after TIPS by Using 4D-Flow MR Imaging. Radiology. 2016;281(2):574–582. [PubMed: 27171019]
30. Frydrychowicz A, Roldan-Alzate A, Winslow E, et al. Comparison of radial 4D Flow-MRI with perivascular ultrasound to quantify blood flow in the abdomen and introduction of a porcine model of pre-hepatic portal hypertension. Eur Radiol. 2017;27(12):5316–5324. [PubMed: 28656461]
31. Roldán-Alzate A, Frydrychowicz A, Niespodzany E, et al. In vivo validation of 4D flow MRI for assessing the hemodynamics of portal hypertension. J Magn Reson Imaging. 2013;37(5):1100–1108. [PubMed: 23148034]

32. Lv T, Kong L, Yang J, et al. The postoperative hepatic artery resistance index after living donor liver transplantation can predict early allograft dysfunction. Medicine (Baltimore). 2020;99(4)https://www.ncbi.nlm.nih.gov/pmc/articles/PMC7004676/. Accessed February 26, 2020.
33. Hypersplenism Peck-Radosavljevic M.. Eur J Gastroenterol Hepatol. 2001;13(4):317–323. [PubMed: 11338057]
34. DuBois B, Mobley D, Chick JFB, Srinivasa RN, Wilcox C, Weintraub J. Efficacy and safety of partial splenic embolization for hypersplenism in pre- and post-liver transplant patients: A 16-year comparative analysis. Clin Imaging. 2019;54:71–77. [PubMed: 30553121]
35. Talwar A, Gabr A, Riaz A, et al. Adverse Events Related to Partial Splenic Embolization for the Treatment of Hypersplenism: A Systematic Review. J Vasc Interv Radiol. 2020;http://www.sciencedirect.com/science/article/pii/S1051044319307031. Accessed February 26, 2020.
36. Keller EJ, Kulik L, Stankovic Z, et al. JOURNAL CLUB: Four-Dimensional Flow MRI–Based Splenic Flow Index for Predicting Cirrhosis-Associated Hypersplenism. Am J Roentgenol. 2017;209(1):46–54. [PubMed: 28463524]
37. Schnell S, Ansari SA, Wu C, et al. Accelerated dual-venc 4D flow MRI for neurovascular applications. J Magn Reson Imaging JMRI. 2017;46(1):102–114. [PubMed: 28152256]
38. Vali A, Aristova M, Vakil P, et al. Semi-automated analysis of 4D flow MRI to assess the hemodynamic impact of intracranial atherosclerotic disease. Magn Reson Med. 2019;82(2):749–762. [PubMed: 30924197]
39. Retson TA, Besser AH, Sall S, Golden D, Hsiao A. Machine Learning and Deep Neural Networks in Thoracic and Cardiovascular Imaging. J Thorac Imaging. 2019;34(3):192–201. [PubMed: 31009397]

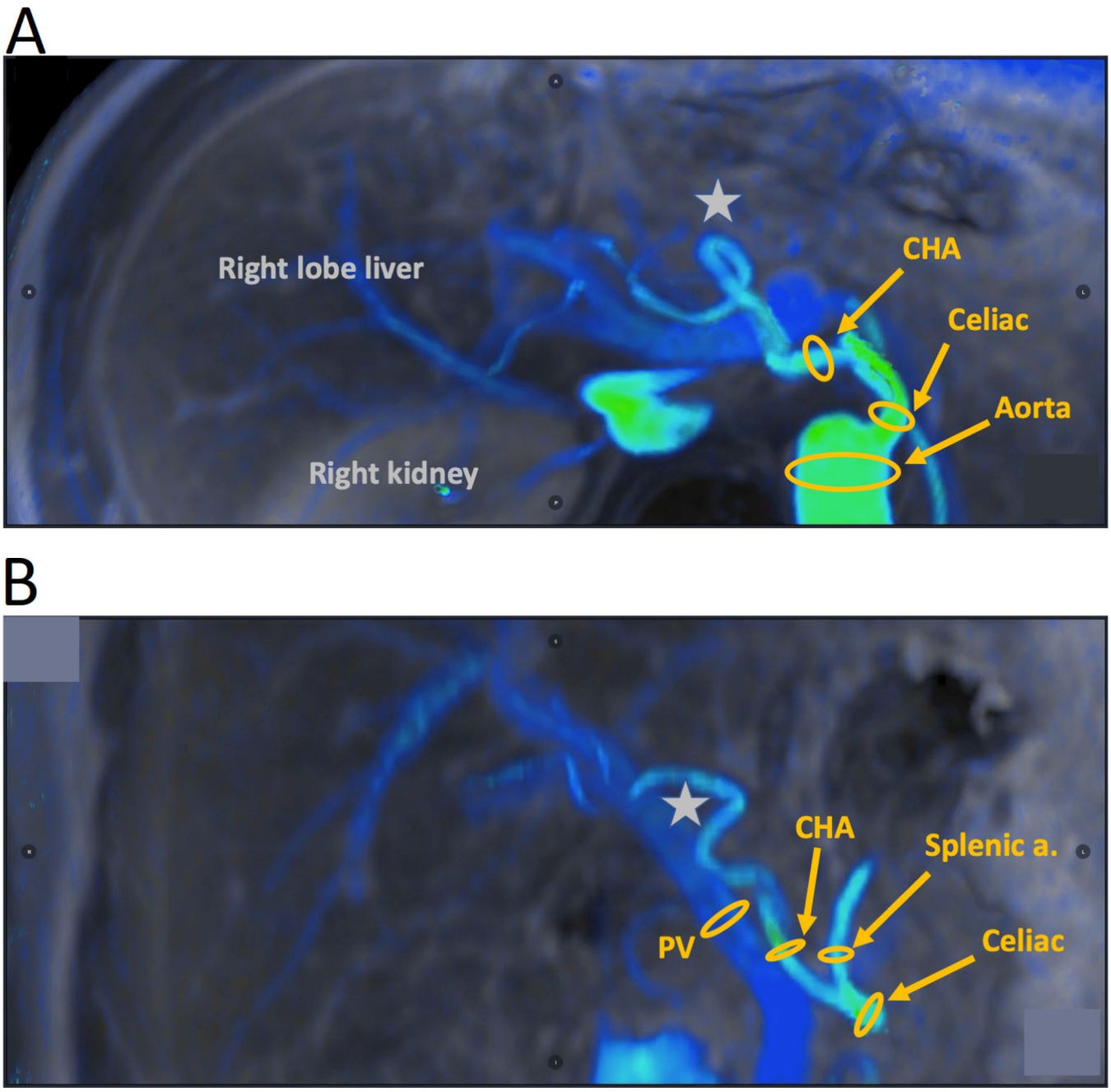

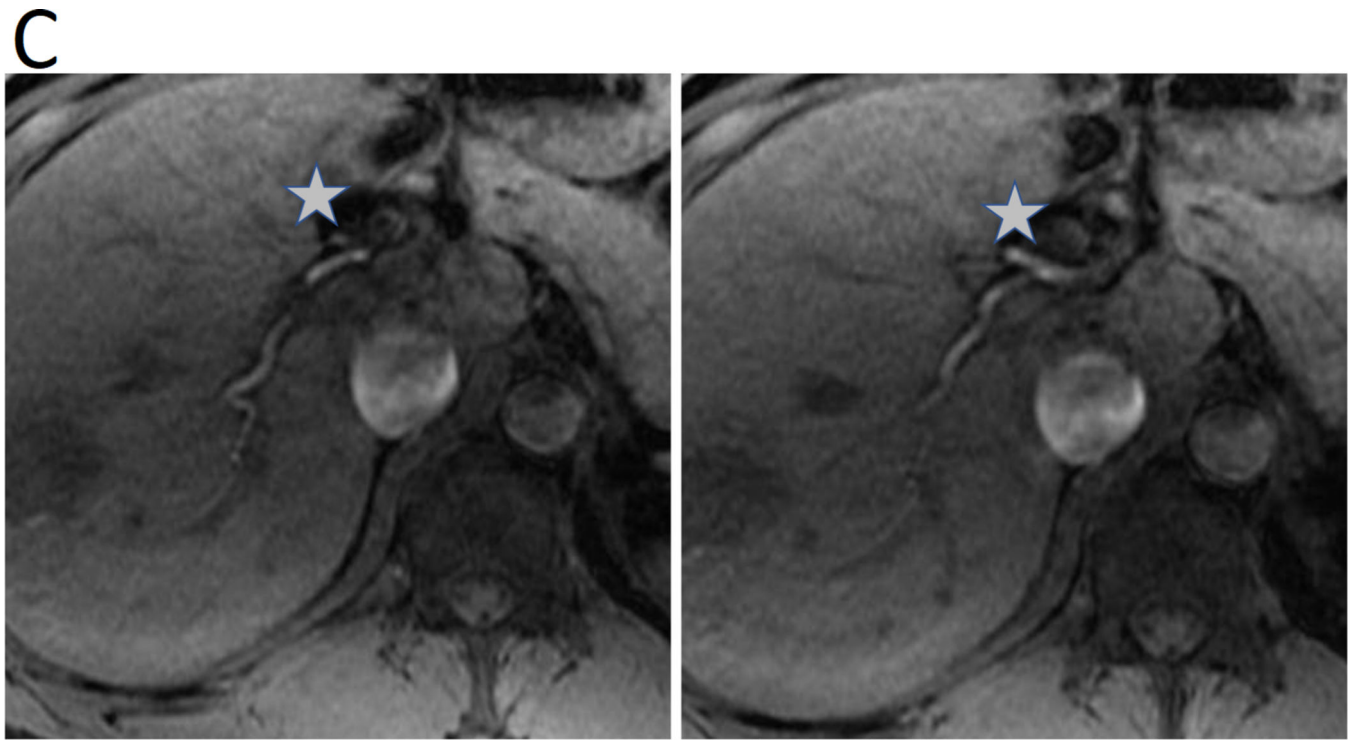

Figure 1: 4D flow with self-navigation and example measurements.

Color coded images at peak systolic flow from a patient with cirrhosis. Blue means slower blood flow while red reflects peak systolic blood flow velocity in the abdominal aorta. (A) Oblique view of 4D flow-SN images showing the course of the celiac trunk and common hepatic artery (CHA) from the aorta into the hepatic hilum (B) Conventional coronal view of 4D flow-SN images showing the bifurcation of the celiac trunk into the splenic artery and CHA, as well at the superior mesenteric vein draining into the portal vein (PV). In both panels A and B, the yellow circles indicate typical location of measurements. (C) Axial T1 weighted imaging showing the course of the proper hepatic and right hepatic arteries. The gray star indicates the location of prominent loop in the proper hepatic artery.

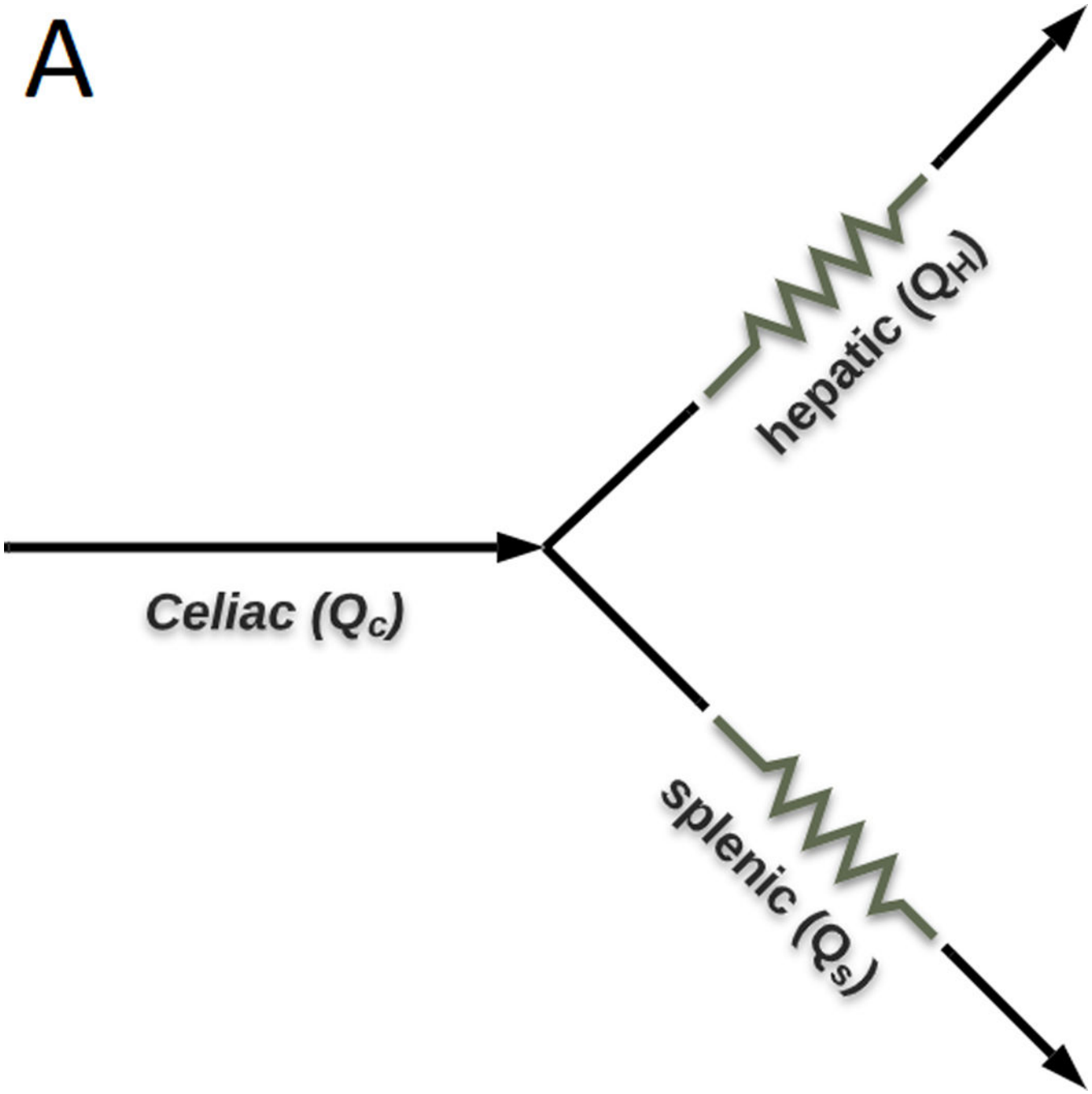

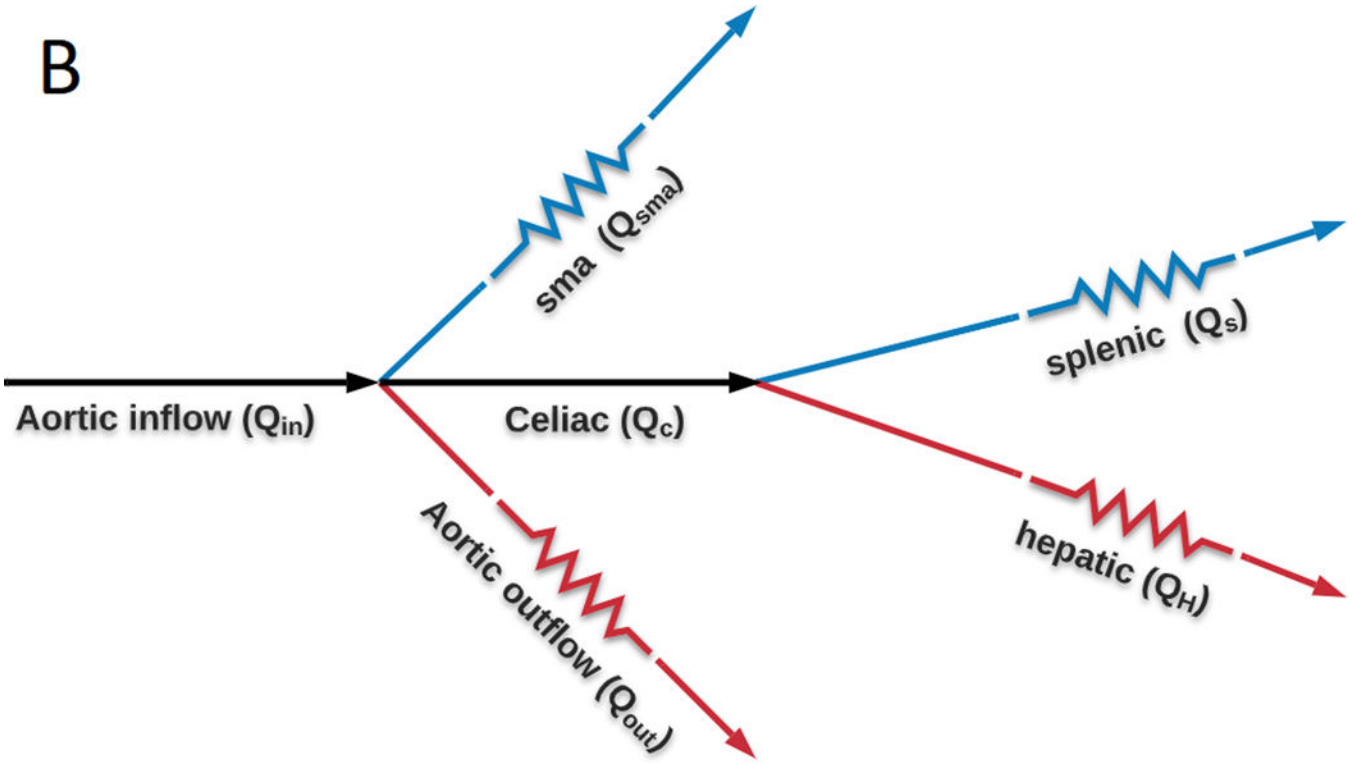

Figure 2: Circuit diagram of HARR and PRI

Panel A: Assuming conventional anatomy and assuming left gastric artery and gastroduodenal artery flow is negligible, blood flow into the celiac trunk splits into the common hepatic artery (Q_H) and the splenic artery (Q_S). Increased resistance in the hepatic artery (R_H) or decreased resistance in the splenic artery (R_s) leads to increased flow in the splenic artery, and vice-versa. Applying Poisuille's relationship yields the hepatic artery relative resistance (HARR) = $(R_H/R_S) = (Q_S/Q_H)$., with Q_S and Q_H being measurable terms using 4D flow.

Panel B: By similar logic to Panel A, we can derive a marker for the resistance of the portal venous system relative to the systemic circulation. Increased resistance in the portal veins will reduce flow in the splenic artery (Q_S) and SMA (Q_{SMA}) while increasing flow in the hepatic artery (Q_H) and aortic outflow (Q_{OUT}) via the suprarenal aorta. Applying Poisuille's relationship yields the portal resistive index (PRI) = $(R_{SMA} + R_S)/(R_{OUT} + R_H) = (Q_{OUT} + Q_H)/(Q_{SMA} + Q_S)$.

SMA = superior mesenteric artery

A

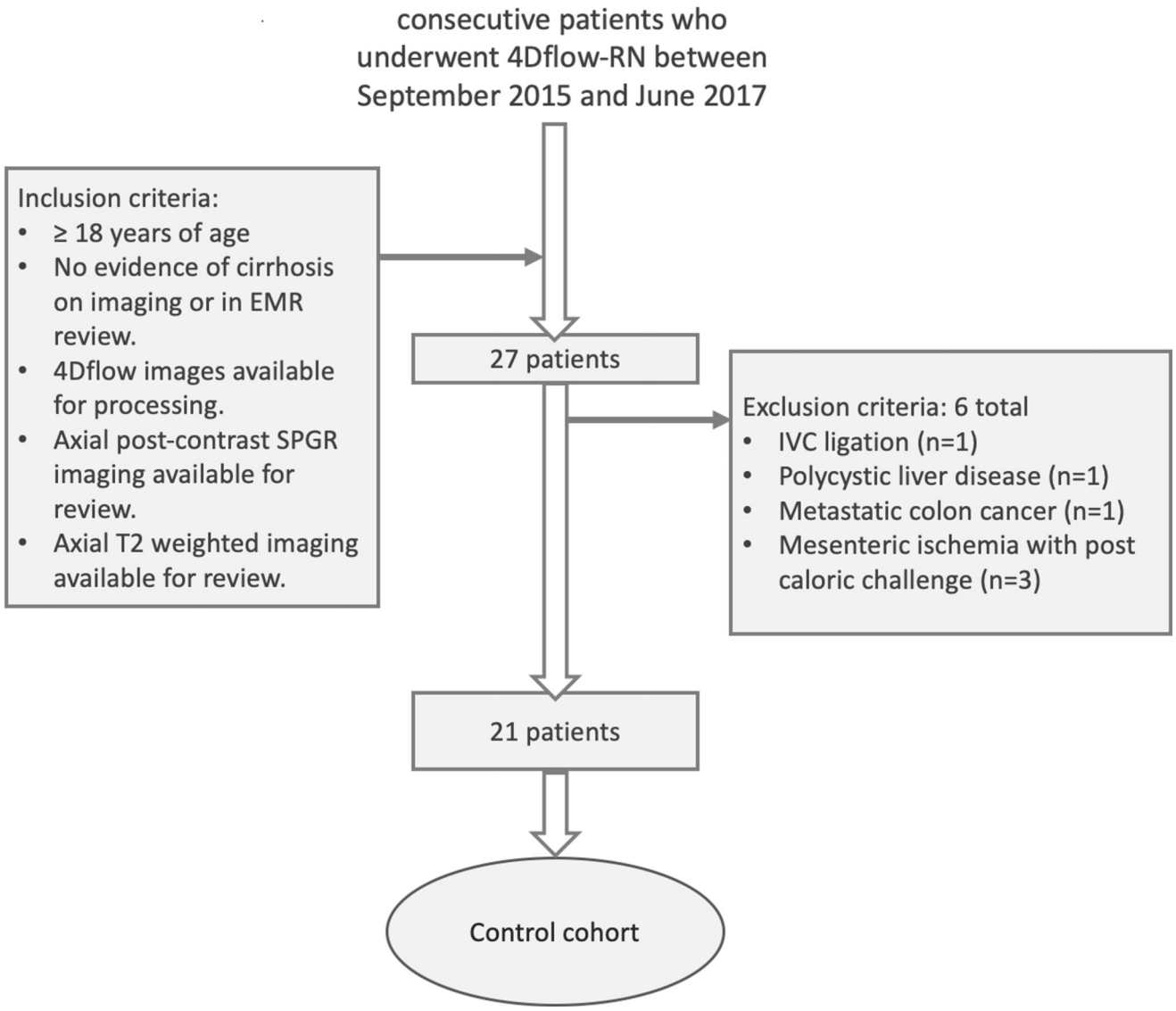

B

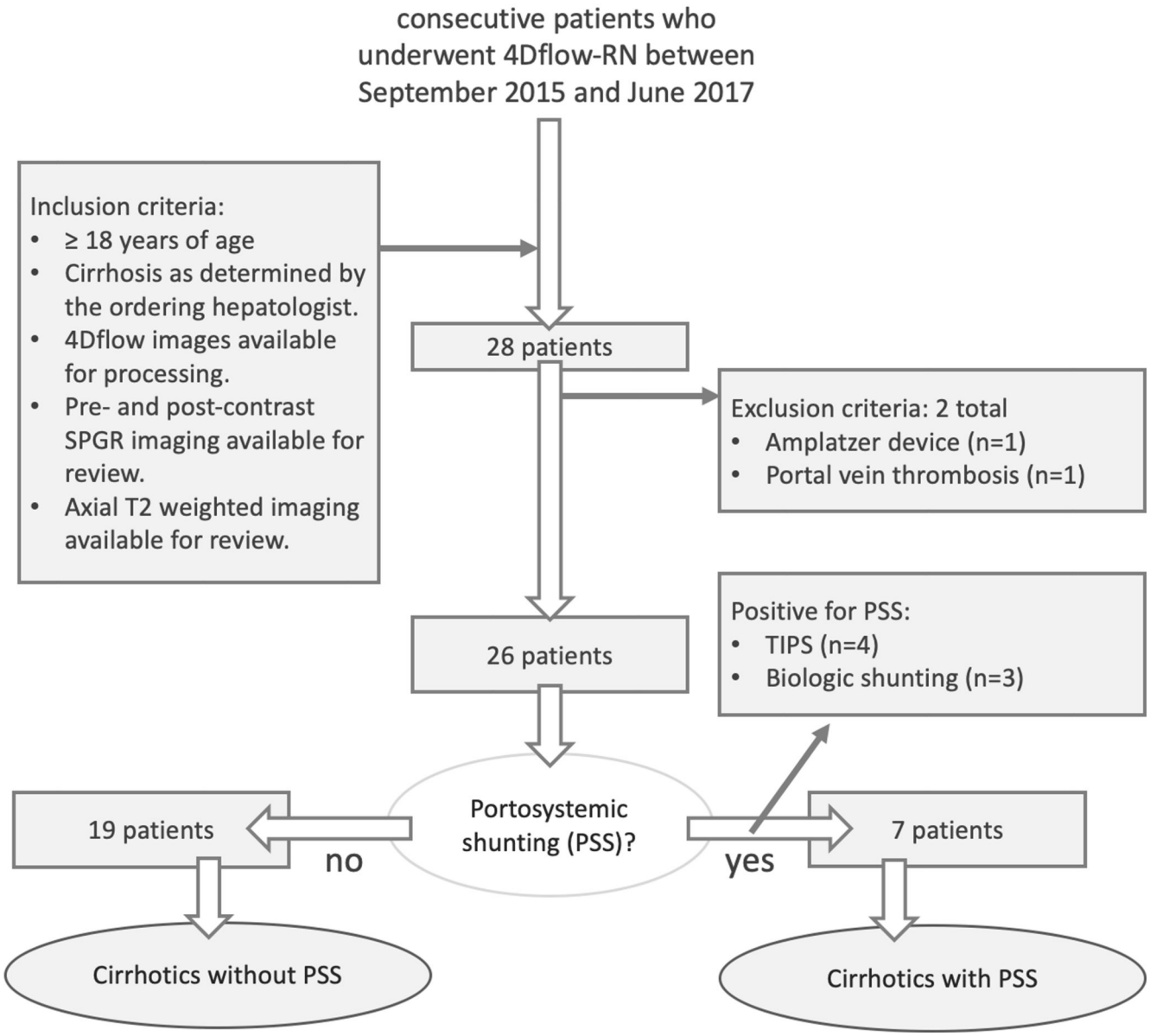

Figure 3: Cohort selection.
Patient flow charts demonstrating selection of patient cohorts.

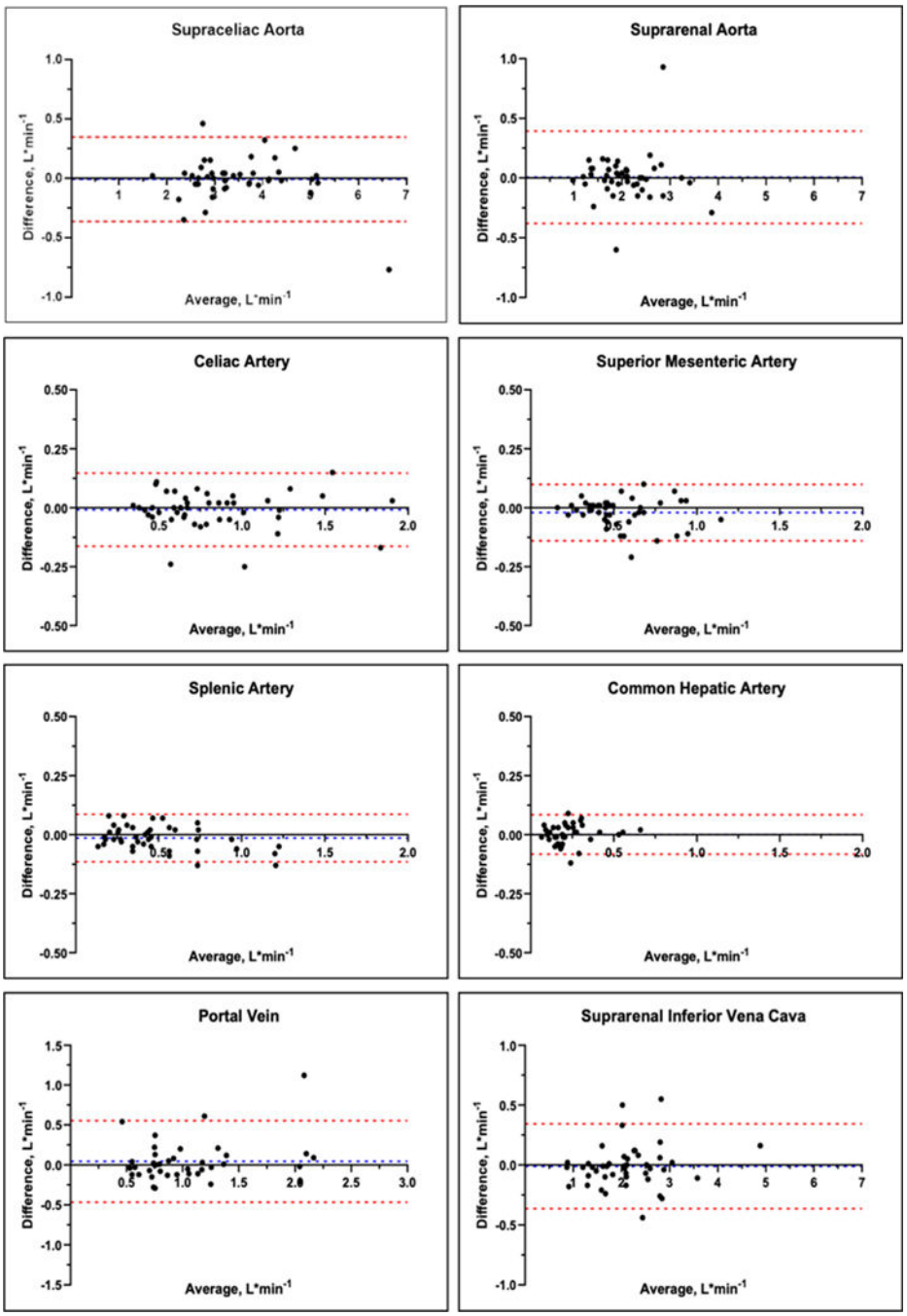

Figure 4: Bland-Altman analysis of inter-reader agreement.

Bland Altman analysis comparing averaged measurements from reader 1 and reader 2 across all vessels.

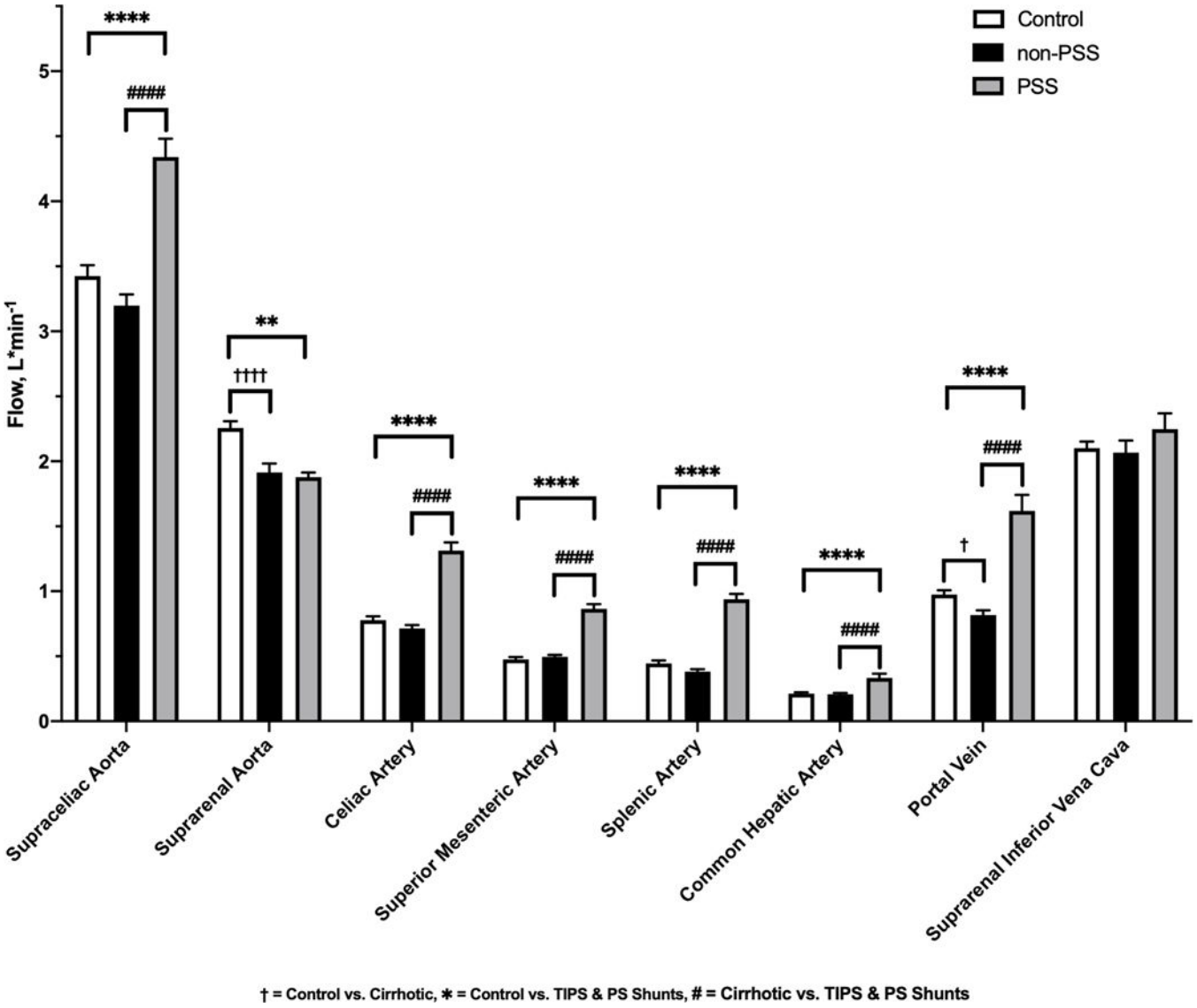

Figure 5: Comparison of blood flow across cohorts.

Quantification of blood flow in the different cohorts across all vessels assessed in the study. Details of p values are provided in Table 4.

**** $p < 0.0001$

** $p < 0.005$

$p < 0.0001$

†††† $p < 0.0001$

† $p < 0.05$

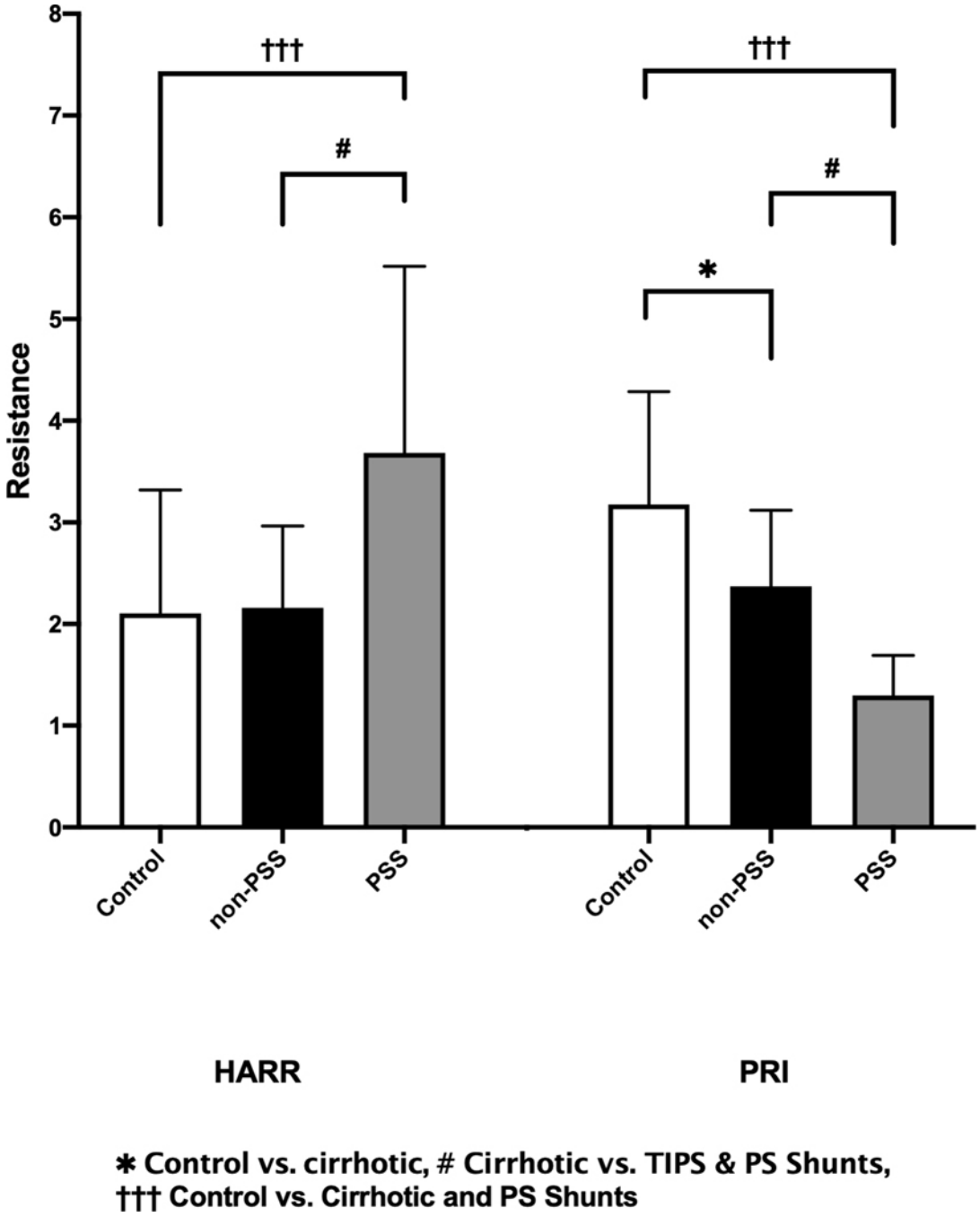

Figure 6: HARR and PRI.

Comparison of hepatic arterial relative resistance (HARR) and portal resistive index (PRI) between the three cohorts of patients: the control cohort, the cirrhosis without portosystemic shunting (non-PSS) cohort, and the cirrhosis with portosystemic shunting (PSS) cohort. HARR was significantly higher in the PSS cohort, as compared to both the control and non-PSS cohort. PRI was significantly reduced in the non-PSS cohort as compared to the control cohort, and the PRI was significantly reduced in the PSS cohort as compared to both other cohorts.

††† $p < 0.05$
# $p < 0.05$
* $p < 0.0005$

Table 1:

4D flow imaging parameters

						Acquisition Matrix			Acquisition Resolution (mm)		
Plane	**#**	**TR (ms)**	**TE (ms)**	**FA**	**BW**	**RL**	**AP**	**IS**	**RL**	**AP**	**IS**
Axial	19	5.15 (4.28 – 5.77)	2.69 (1.92 – 3.14)	15	62 – 63	192 – 256	120 – 192	40 – 120	1.3 – 2.0	1.7 – 2.4	1.3 – 4.0
Coronal	27	5.39 (5.03 – 5.62)	2.85 (2.60 – 3.03)	15	62	192	60 – 90	224 – 256	2.0 – 2.5	2.8 – 3.2	1.5 – 2.1
Sagittal	1	5.54	2.9	15	62	60	192	256	2.8	2.0	1.5

						Acceleration	
Plane	**#**	**Scan time (min:sec)**	**Venc (cm/s)**	**Heartrate (bpm)**	**Temporal Resolution (ms)**	**In plane**	**Through plane**
Axial	19	9:56 (6:48 – 14:47)	80 (80 – 250)	67 (18–103)	51 (29–167)	1.8 (1.6 – 3.0)	2.0 (1.6 × 2.2)
Coronal	27	10:09 (7:57 – 11:56)	120 (100 – 200)	71 (47–91)	43 (33–64)	3.2 (2.0 – 3.2)	2.0 (1.3 × 2.0)
Sagittal	1	11:31	150	68	44	2.0	2.0

TABLE 2:

Summary of Per Vessel Blood Flow Analysis

	Reader						Statistical analysis[e]				
	1			2				Bland-Altman		Linear Regression	
Vessel	**#[a]**	**ave (±SD)[b,c]**	**range[b,d]**	**#[a]**	**ave (±SD)[b,c]**	**range[b,d]**	**#[f]**	**bias[b]**	**95% CI[b]**	**r**	**R^2**
SC Aorta	44/47 (94%)	3.46 (±0.08)	1.71 – 6.25	44/47 (94%)	3.47 (±0.09)	1.69 – 7.02	44	−0.01	−0.37 – 0.35	0.984	0.967
SR Aorta	44/47 (94%)	2.09 (±0.06)	0.97 – 3.72	44/47 (94%)	2.07 (±0.05)	0.99 – 4.01	44	< 0.01	−0.38 – 0.39	0.949	0.901
Celiac	44/47 (94%)	0.82 (±0.05)	0.35 – 1.92	44/47 (94%)	0.83 (±0.04)	0.34 – 1.92	44	< −0.01	−0.16 – 0.15	0.978	0.956
SMA	44/47 (94%)	0.53 (±0.04)	0.16 – 1.12	44/47 (94%)	0.55 (±0.03)	0.16 – 1.17	44	−0.02	−0.14 – 0.10	0.962	0.925
Splenic	43/47 (91%)	0.48 (±0.04)	0.11 – 1.20	43/47 (91%)	0.50 (±0.03)	0.16 – 1.27	42	−0.01	−0.11 – 0.09	0.987	0.974
CHA	40/47 (85%)	0.23 (±0.02)	0.06 – 0.67	43/47 (91%)	0.22 (±0.02)	0.06 – 0.65	39	< 0.01	−0.08 – 0.08	0.948	0.900
PV	42/47 (89%)	1.02 (±0.06)	0.22 – 2.64	40/47(85%)	1.01 (±0.05)	0.19 – 2.15	39	0.04	−0.47 – 0.55	0.866	0.751
SR IVC	44/47 (94%)	2.10 (±0.07)	0.82 – 4.96	44/47 (94%)	2.11 (±0.09)	0.87 – 4.80	44	−0.01	−0.36 – 0.34	0.972	0.945

a: number of cases where vessel listed interpreted as measurable – listed by reader;

b: values are blood flow in liters per minute;

c: average value from all measurements for all patients in the listed vessel, and average standard deviation for all patients – listed by reader;

d: range of per patient mean values from triplicate measurements – listed by reader;

e: assessment of inter-reader correlation, the mean value from the triplicate measurement from each reader was used in the analysis;

f: number of cases that were deemed measurable by both readers and thus were used for statistical analysis.

Abbreviations: SC Aorta = supraceliac abdominal aorta; SR Aorta = suprarenal abdominal aorta; Celiac = celiac trunk; SMA = superior mesenteric artery; Splenic = splenic artery; CHA = common hepatic artery; PV = portal vein; SR IVC = suprarenal inferior vena cava; SD = standard deviation

TABLE 3:

Conservation of Flow Analysis

		Bland-Altman		Linear Regression	
Vessel	**#**[a]	**bias**[b]	**95% CI**[b]	**r**	**R^2**
SC Aorta - SR Aorta = Celiac + SMA	42	0.026	−0.474 – 0.526	0.909	0.825
Celiac + SMA = PV	39	0.311	−0.242 – 0.864	0.862	0.744
Celiac = CHA + Splenic	39	0.106	−0.130 – 0.342	0.939	0.882
SR Aorta = SR IVC	44	−0.034	−0.910 – 0.843	0.806	0.649

a: number of patients with adequate data for inclusion in the analysis;

b: numbers represent blood flow in liters per minute.

Abbreviations: SC Aorta = supraceliac abdominal aorta; SR Aorta = suprarenal abdominal aorta; Celiac = celiac trunk; SMA = superior mesenteric artery; Splenic = splenic artery; CHA = common hepatic artery; PV = portal vein; SR IVC = suprarenal inferior vena cava

TABLE 4:

Summary of Grouped Analysis

	A: Controls			B: Cirrhotics w/o PSS			C: Cirrhotics with PSS			Differences in flow		
	21 patients[a]			17 patients[a]			6 patients[a]			A-B	C-A	C-B
Vessel	**Ave[b]**	**SEM[b]**	**n[c]**	**Ave[b]**	**SEM[b]**	**n[c]**	**Ave[b]**	**SEM[b]**	**n[c]**	**Diff[d] (95% CI) p value[d]**	**Diff[d] (95% CI) p value[d]**	**Diff[d] (95% CI) p value[d]**
SC Aorta	3.43	0.8	126	3.20	0.09	102	4.34	0.14	36	0.23 (−0.05 – 0.51) p = 0.1405	0.91 (0.51 – 1.32) ***p < 0.0001***	1.14 (0.73 – 1.56) ***p < 0.0001***
SR Aorta	2.26	0.05	125	1.91	0.07	102	1.88	0.04	36	0.34 (0.16 – 0.53) ***p < 0.0001***	−0.37 (−0.16 – −0.53) ***p = 0.0026***	−0.04 (−0.24 – 03.31) p = 0.9498
Celiac	0.78	0.03	126	0.71	0.03	102	1.31	0.06	36	0.06 (−0.04 – 0.16) p =0.2843	0.54 (0.39 – 0.69) ***p < 0.0001***	0.60 (0.45 – 0.75) ***p < 0.0001***
SMA	0.48	0.02	126	0.50	0.01	102	0.87	0.04	36	−0.02 (−0.07 – 0.04) p = 0.7126	0.39 (0.31 – 0.47) ***p < 0.0001***	0.37 (0.29 – 0.45) ***p < 0.0001***
Splenic	0.44	0.02	123	0.38	0.02	99	0.94	0.04	36	0.06 (−0.01 – 0.13) p = 0.1117	0.49 (0.39 – 0.59) ***p < 0.0001***	0.56 (0.45 – 0.66) ***p < 0.0001***
CHA	0.21	0.01	117	0.21	0.01	96	0.31	0.03	36	0.01 (−0.03 – 0.05) p = 0.9467	0.12 (0.07 – 0.18) ***p < 0.0001***	0.13 (0.07 – 0.18) ***p < 0.0001***
PV	0.97	0.03	120	0.82	0.03	90	1.62	0.12	36	0.16 (0.02 – 0.30) ***p = 0.024***	0.64 (0.45 – 0.84) ***p < 0.0001***	0.80 (0.60 – 1.00) ***p < 0.0001***
SR IVC	2.10	0.05	126	2.07	0.09	102	2.25	0.12	36	0.02 (−0.20 – 0.27) p =0.9397	0.15 (−0.19 – 0.49) p = 0.5551	0.18 (−0.16 – 0.53) p = 0.4305

a: the three patients without any measurements were excluded from analysis;

b: measurements are in liters of blood flow per minute;

c: this is the sum total number of measurements from both readers, some vessels were not measurable in some patients, and in one control patient the SR Aorta was measured in duplicate rather than triplicate, resulting in 125 rather than 126 measurements;

d: the p values were calculated using Tukey's multiple comparison test,

$p < 0.05$ was considered significant and is indicated in ***bold italics***